Supplementary Information (SI) Appendix for

Widespread decline in winds delayed autumn foliar senescence over high latitudes

Chaoyang Wu[1, 2*], Jian Wang[3*], Philippe Ciais[4], Josep Peñuelas[5,6], Xiaoyang Zhang[7], Oliver Sonnentag[8], Feng Tian[9], Xiaoyue Wang[1, 2], Huanjiong Wang[1, 2], Ronggao Liu[1, 2], Yongshuo H. Fu[10], Quansheng Ge[1, 2*]

1. The Key Laboratory of Land Surface Pattern and Simulation, Institute of Geographical Sciences and Natural Resources Research, Chinese Academy of Sciences, Beijing 100101, China;
2. University of the Chinese Academy of Sciences, Beijing 100049, China;
3. Department of Geography, The Ohio State University, Columbus, OH 43210, USA;
4. Laboratoire des Sciences du Climat et de l'Environnement, IPSL-LSCE CEA CNRS UVSQ, 91191, Gif sur, Yvette, France;
5. CSIC, Global Ecology Unit CREAF-CSIC-UAB, Bellaterra, Barcelona 08193, Catalonia, Spain;
6. CREAF, Cerdanyola del Valles, Barcelona 08193, Catalonia, Spain;
7. Geospatial Sciences Center of Excellence (GSCE), Department of Geography, South Dakota State University, 1021 Medary Ave., Wecota Hall 506B, Brookings, SD 57007-3510, USA;
8. Département de géographie and Centre d'études nordiques, Université de Montréal, Montréal, QC H2V 2B8, Canada;
9. School of Remote Sensing and Information Engineering, Wuhan University, Wuhan 430079, China;
10. College of Water Sciences, Beijing Normal University, Beijing 100875, China;

***Corresponding authors:** C Wu (wucy@igsnrr.ac.cn), J Wang (wang.12679@osu.edu), and Q Ge (geqs@igsnrr.ac.cn).

This PDF file includes:
Supplementary Explanation
Figs. E1 to E3
Supplementary Tables and Figures
Figs. S1 to S8
Tables S1 to S3

Explanation

Explanation 1 Reasons for region determination

Declined winds were reported worldwide, especially at high latitudes. We first detected the temporal trend of wind speed over mid to high latitude (>30°N, Fig. E1). We noted that for regions in 30-46°N, the average trend of wind speed is close to 0, while for regions above 46°N, a decreasing trend becomes dominant (Fig. E1*A*). In addition, we also calculated the ratio of pixels with decreasing trend of wind speed to those with increasing trend is above 1 over regions above 48°N (Fig. E1*B*). Above all, we restricted our study areas at latitudes >50°N to investigate the response of autumn DFS to lower wind speed in high latitudes.

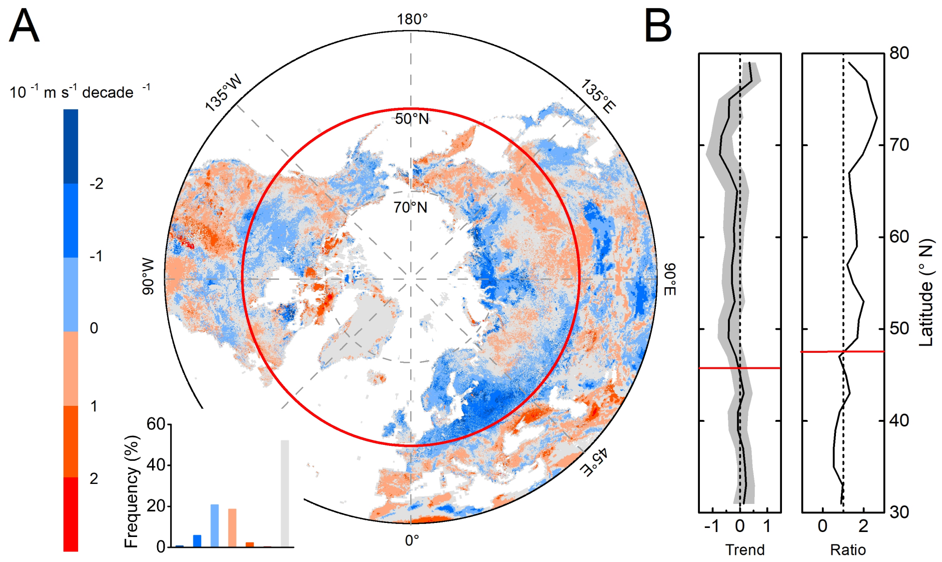

Fig. E1. Temporal trend of wind speed for mid to high latitudes (>30°). *A* represents spatial distribution of wind speed trend. *B* represents wind speed trend based on latitudinal profiles (left) and the ratio of pixels with decreasing wind speed trend and those with increasing trend (right). Significance was set at $P < 0.05$. Non-significant pixels were showed in gray.

Explanation 2 Impacts of temperature uncertainty

For meteorological data of temperature, precipitation and radiation, we used the CRU-TS 4.00 datasets. We recognize that these data have weakness over high latitude regions, yet these data may be the best choice currently available given that weather stations are indeed scarce for those regions. We here provide several reasons that help to alleviate concerns from applying these gridded data in our analyses.

First, these meteorological data have been tested and validated over these regions (Brohan et al., 2006). There are 580 stations (Fig. E2) for CRU datasets over high northern latitudes (>50°). For ground analysis in Europe, we used meteorological variables extracted from CRU datasets where there are dense land stations (>200 sites), thus, to some degree, alleviating associated uncertainty.

Second, although the data have limitations, it is still useful for the scientific community to analyze interactions between climate change and vegetation activities. For example, several studies used these datasets to explore the relationships of plant phenological changes with climate (Piao et al., 2014, Fu et al., 2015, Piao et al., 2015).

Third, instead of the absolute values, we focused on the temporal trends of these meteorological data in our analysis. We here also compared the trend of temperature, precipitation, and cloud cover (a proxy of solar radiation), derived from CRU and ERA. We observed high similarity of trends between the two datasets (Fig. E3), especially for temperature that is widely reported to influence DFS.

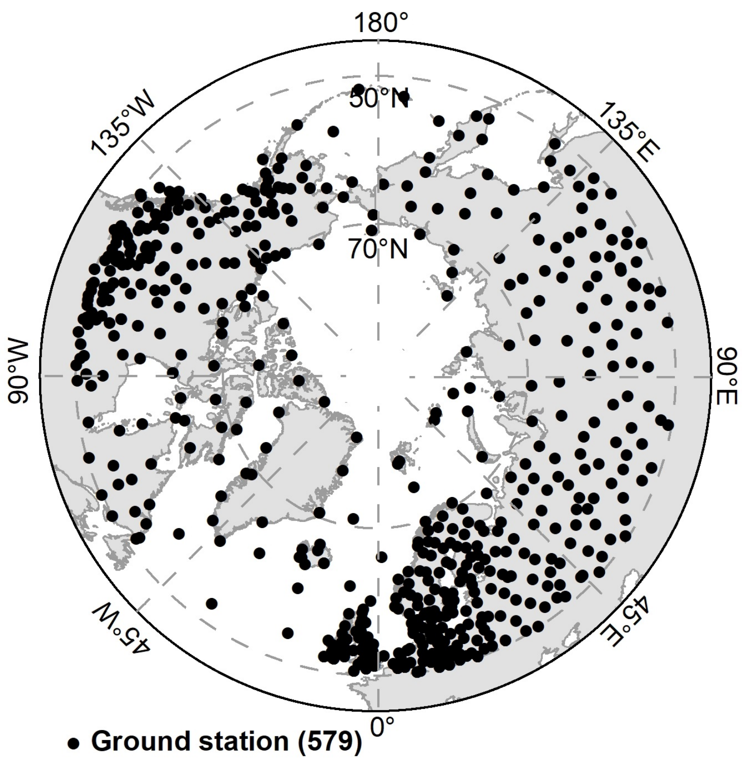

Fig. E2. Land station coverage for CRU datasets over high norther latitudes (>50°), also see Brohan et al., 2006.

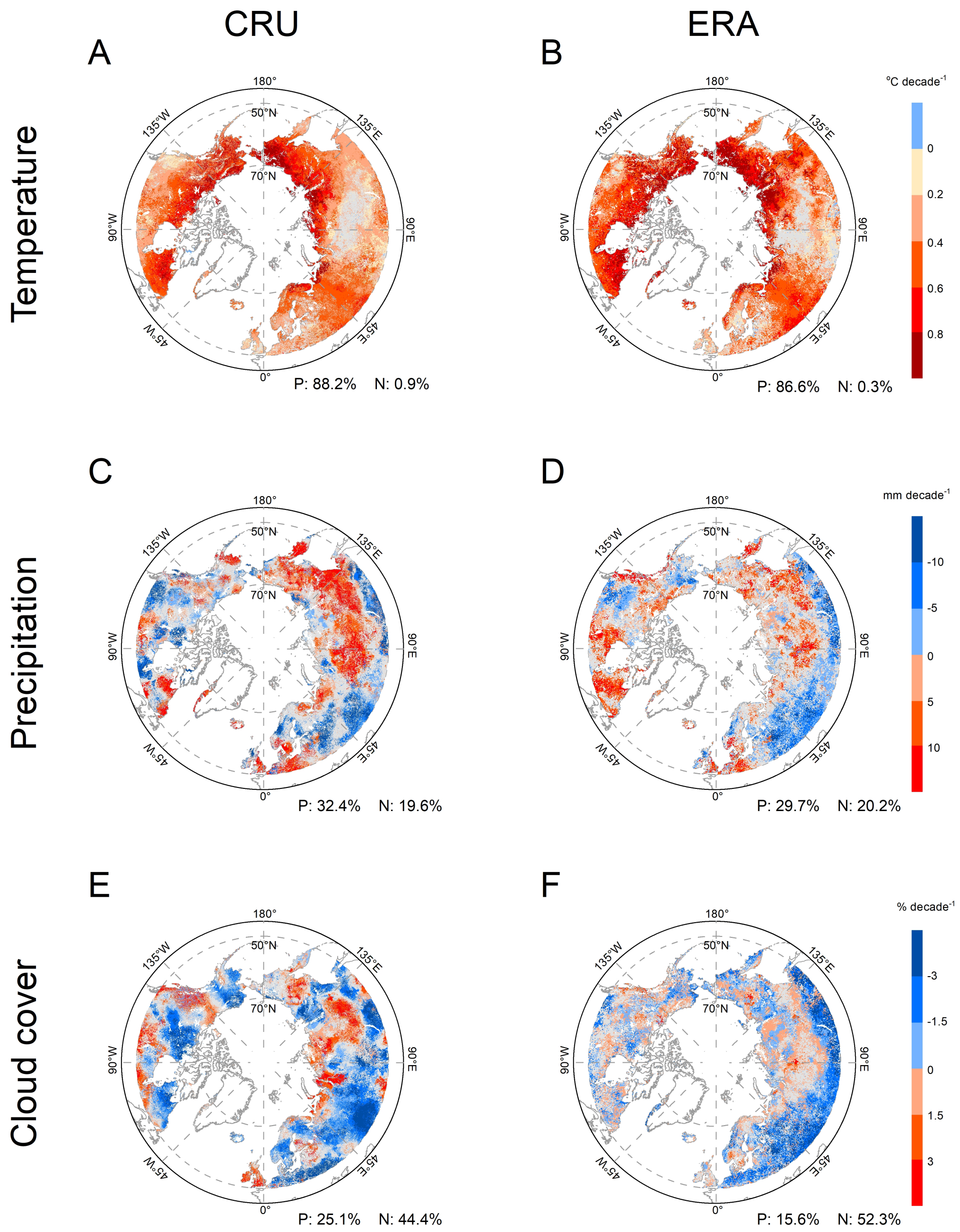

Fig. E3. Temporal trends of meteorological factors for 1982-2015 at high latitudes. *A* and *B* represent temporal trends of temperature (°C decade^{-1}), derived from (*A*) CRU and (*B*) ERA, respectively. *C* and *D* represent temporal trends of precipitation (mm decade^{-1}), derived from (*C*) CRU and (*D*) ERA, respectively. *E* and *F* represent temporal trends of cloud cover (% decade^{-1}), derived from (*E*) CRU and (*F*) ERA, respectively. Significance was set at $P < 0.05$. Non-significant pixels were showed in gray.

References:

Brohan P, et al. (2006) Uncertainty estimates in regional and global observed temperature changes: A new dataset from 1850. *J Geophys Res* **111**:D12106.

Piao S, et al. (2014) Evidence for a weakening relationship between interannual temperature variability and northern vegetation activity. *Nat Commun* **5**:5018.

Fu Y, et al. (2015) Declining global warming effects on the phenology of spring leaf unfolding. *Nature* **526**:104–107.

Piao S, et al. (2015) Leaf onset in the northern hemisphere triggered by daytime temperature. *Nat Commun* **6**:6911.

Supplementary Tables and Figures

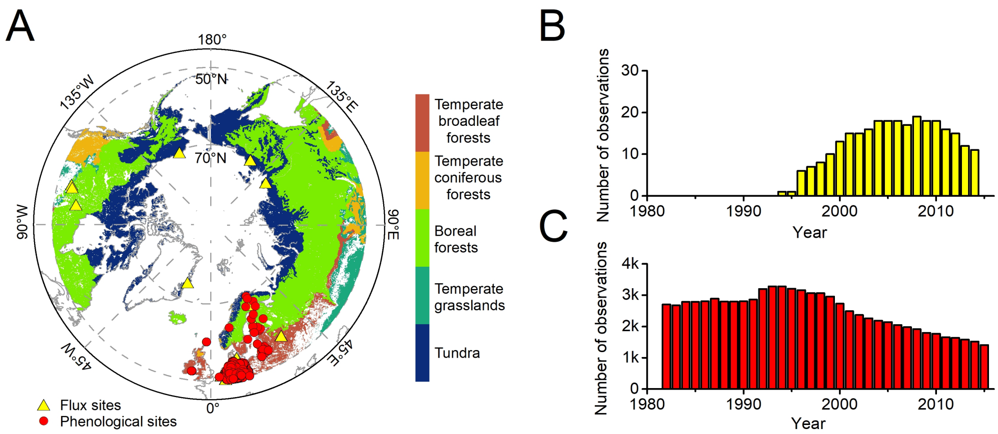

Fig. S1. Spatial distributions of the observational sites. A represents geographic region and the locations of the flux sites and ground phenological sites. B and C represent the number of observations each year for 1982-2015 of flux sites and phenological sites, respectively.

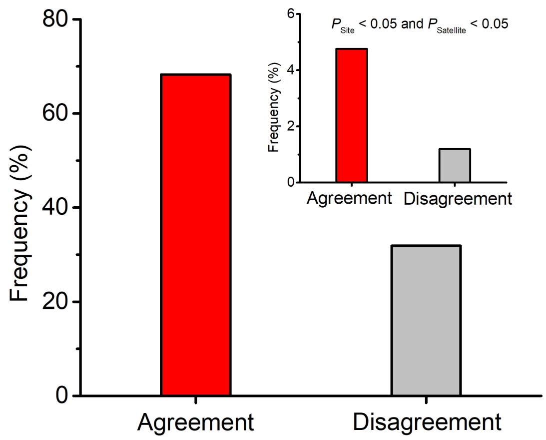

Fig. S2. Percentage of consistency (agreement) and inconsistency (disagreement) of correlation between site- and satellite-based partial correlation.

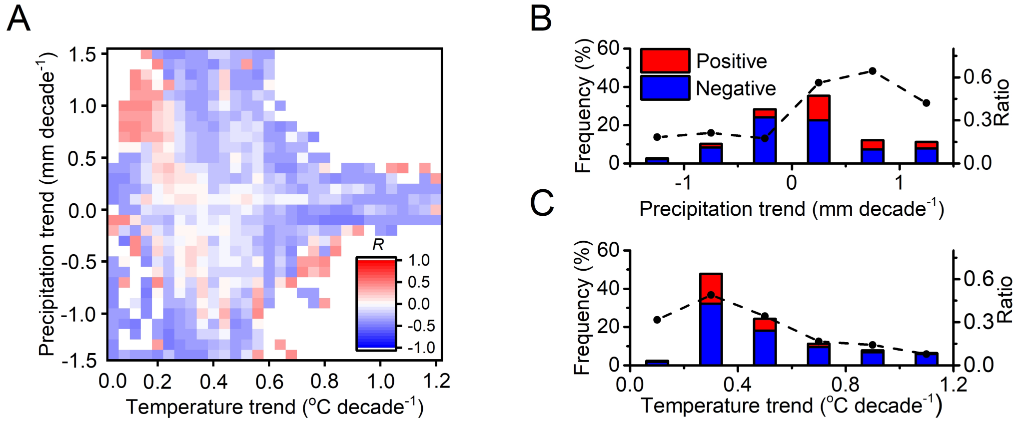

Fig. S3. Distribution of partial correlation between wind speed and dates of autumn foliar senescence (DFS). A represents variations of partial correlation along temperature and precipitation trend gradients. B and C represent distribution of significantly positive and negative partial correlation under different trends of precipitation and temperature, respectively.

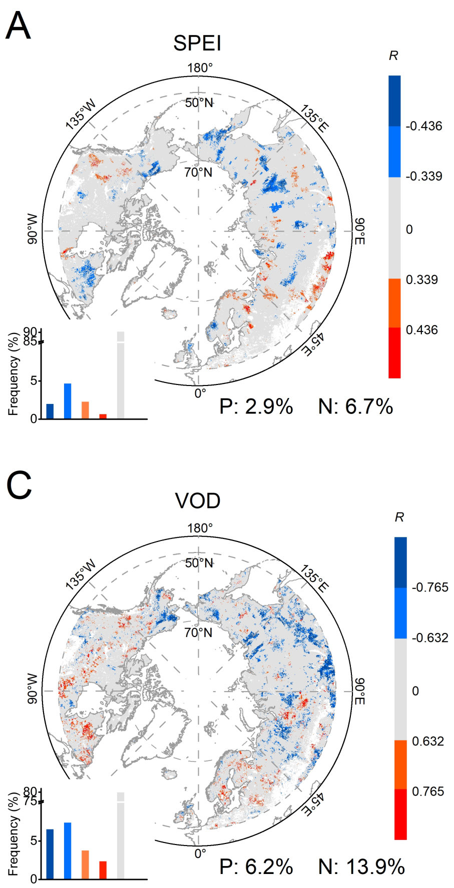

Fig. S4. Partial correlation between wind speed and water indicators. A, B, and C represent partial correlation between wind speed and the Standardized Precipitation Evapotranspiration Index (SPEI, 1982-2015), the Palmer Drought Severity Index (PDSI, 1982-2015), and the Vegetation Optical Depth (VOD, 2002-2011), respectively. The grey color in C represents non-significant correlation. Significance was set at $P < 0.05$.

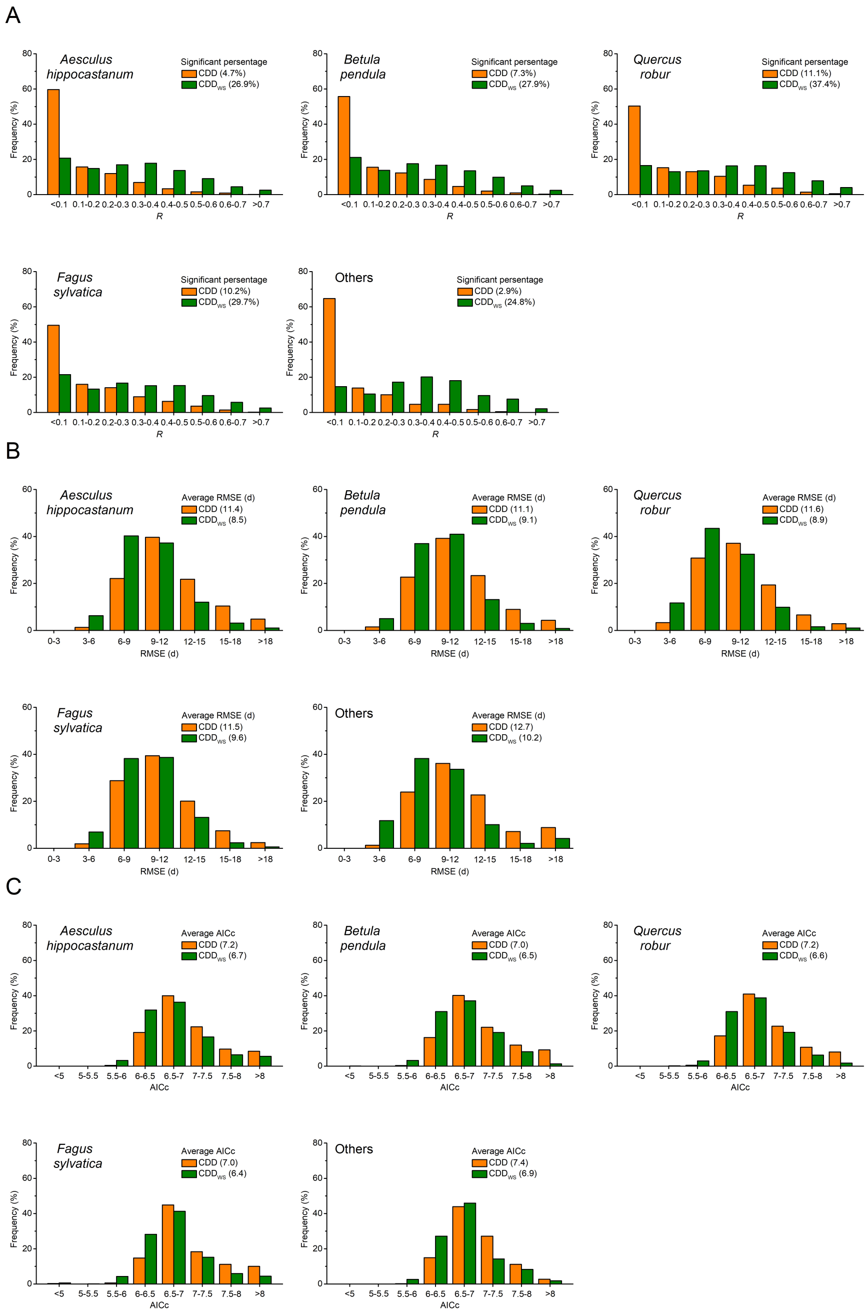

Fig. S5. Comparison between traditional cooling degree days (CDD) and CDD with wind speed (CDD_{WS}) for dates of autumn foliar senescence (DFS) modeled using ground data. A, B and C represent *R*, root mean square error (RMSE) and the corrected Akaike information criterion (AICc). Significance was set at $P < 0.05$.

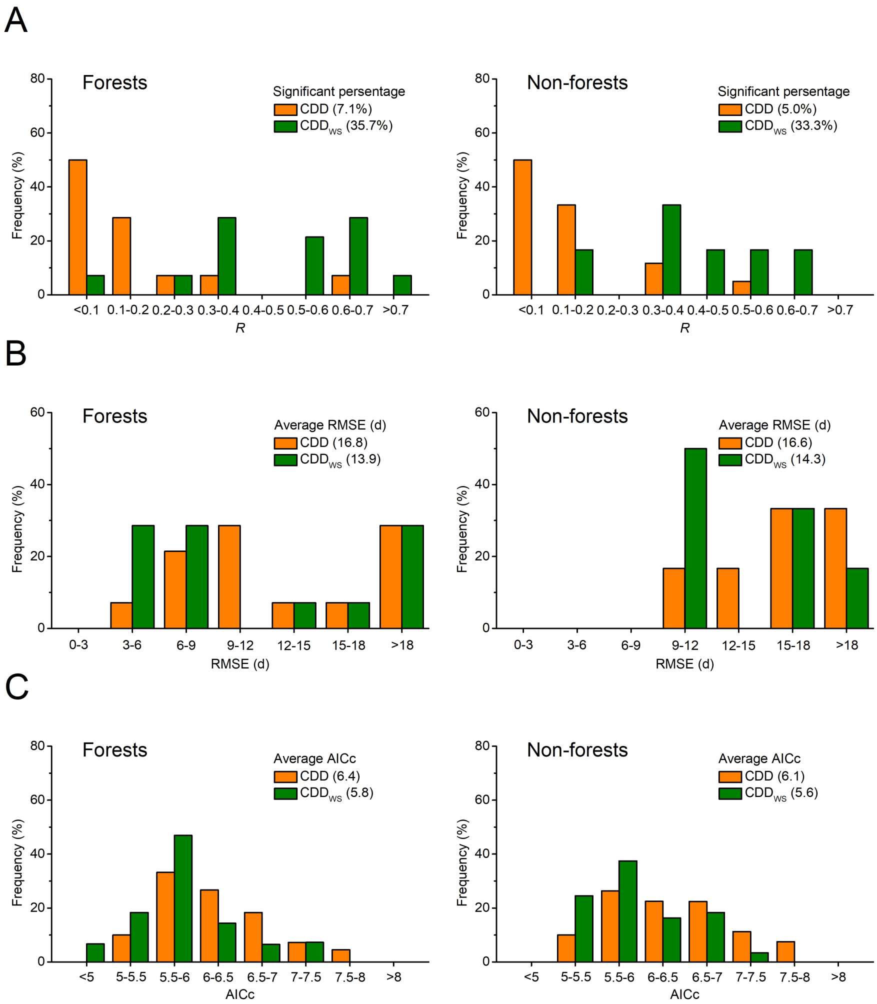

Fig. S6. Comparison between traditional cooling degree days (CDD) and CDD with wind speed (CDD_{WS}) for dates of autumn foliar senescence (DFS) modeled using flux data. A, B and C represent *R*, root mean square error (RMSE) and the corrected Akaike information criterion (AICc). Significance was set at $P < 0.05$.

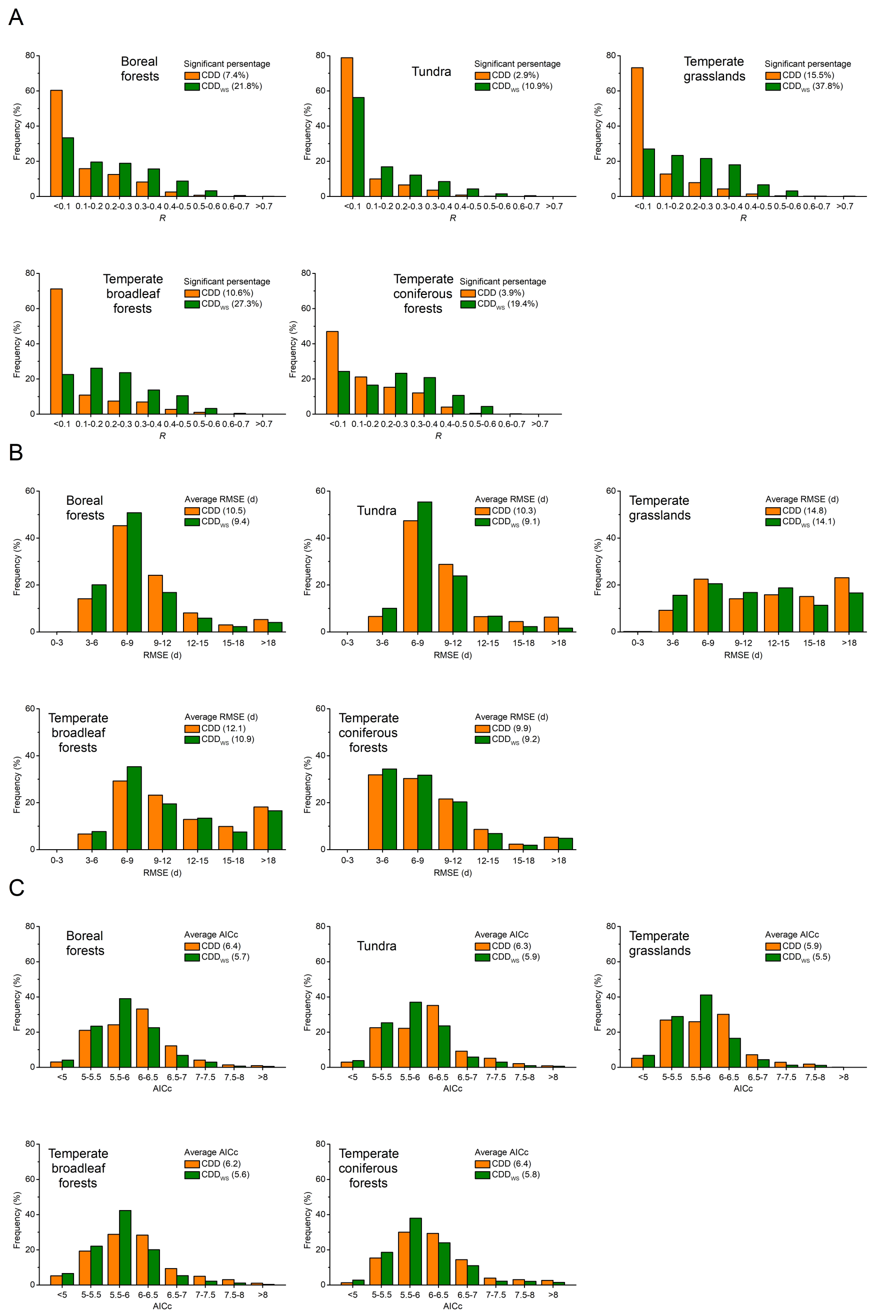

Fig. S7. Comparison between traditional cooling degree days (CDD) and CDD with wind speed (CDD_{WS}) for dates of autumn foliar senescence (DFS) modeled using NDVI3g data. A, B and C represent R, root mean square error (RMSE) and the corrected Akaike information criterion (AICc). Significance was set at $P < 0.05$.

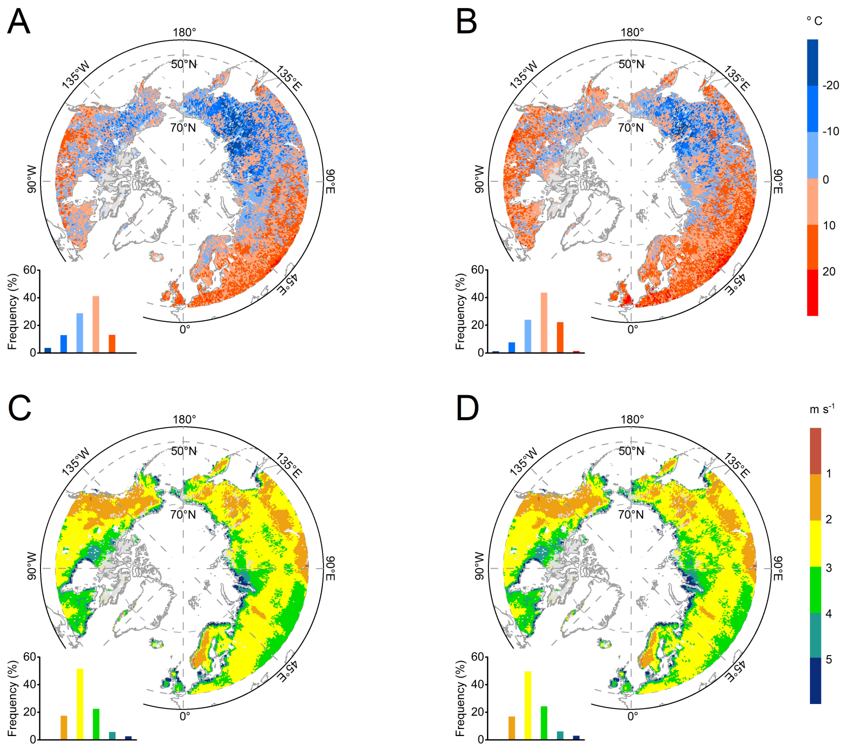

Fig. S8. Projections of average temperature and wind speed for scenarios of representative concentration pathways (RCPs) RCP 4.5 and RCP 8.5. (A) temperature for RCP 4.5, (B) temperature for RCP 8.5, (C) wind speed for RCP 4.5, (D) wind speed for RCP 8.5.

Table S1 Summary of data used in this study.

	Data	Unit	Spatial resolution	Temporal resolution	Time range	Source
Phenology data	DFS	DOY	-	Yearly	1982-2015	PEP725[1]
	GPP	g m^{-2} d^{-1}	-	Daily	1994-2014	FLUXNET[2]
	NDVI	-	1/12°	16 days	1982-2015	GIMMS3g[3]
Climatic data	WS	m s^{-1}	1/24°	Monthly	1982-2015	TerraClimate[4]
	WS	m s^{-1}	0.25°	Monthly	1982-2015	ERA5-Land[5]
	TMP	°C	0.5°	Monthly	1982-2015	CRU-TS 4.00[6]
	PRE	mm	0.5°	Monthly	1982-2015	CRU-TS 4.00[6]
	CLD	-	0.5°	Monthly	1982-2015	CRU-TS 4.00[6]
Water indicators	SM_S	%	0.25°	Monthly	1982-2015	C3S[5]
	SM_V	m^3 m^{-3}	0.25°	Monthly	1982-2015	C3S[5]
	T_{dew}	°C	0.1°	Monthly	1982-2015	ERA5-Land[5]
	SPEI	-	0.5°	Monthly	1982-2015	CSIC[7]
	PDSI	-	1/24°	Monthly	1982-2015	TerraClimate[4]
	VOD	-	0.25°	Monthly	2002-2011	LPDR v2[8]
Model inputs	WS	m s^{-1}	0.5°	Daily	1982-2015	GLADS[9]
	TMP	°C	0.5°	Daily	1982-2015	ESRL-NOAA[10]
	WS-RCP 4.5	m s^{-1}	0.5°	Daily	2081-2100	CCSM[11]
	WS-RCP 8.5	m s^{-1}	0.5°	Daily	2081-2100	CCSM[11]
	TMP-RCP 4.5	°C	0.5°	Daily	2081-2100	CCSM[11]

	TMP-RCP 8.5	°C	0.5°	daily	2081-2100	CCSM[11]

DFS: date of autumn foliar senescence; GPP: gross primary productivity; NDVI: normalized difference of vegetation index; WS: wind speed; TMP: mean air temperature; PRE: precipitation; CLD: cloud cover; SM_S: soil moisture saturation; SM_V: volumetric surface soil moisture; T_{dew}: dew point temperature; SPEI: standardized precipitation evapotranspiration index; PDSI: Palmer drought severity index; VOD: vegetation optical depth; RCP: representative concentration pathway.

Corresponding data availability:

1. http://www.pep725.eu/
2. https://fluxnet.org/
3. https://ecocast.arc.nasa.gov/data/pub/gimms/
4. http://www.climatologylab.org/terraclimate.html
5. https://cds.climate.copernicus.eu/
6. https://sites.uea.ac.uk/
7. http://spei.csic.es/database.html
8. http://files.ntsg.umt.edu/data/LPDR_v2/
9. https://ldas.gsfc.nasa.gov/gldas/
10. https://psl.noaa.gov/
11. https://esgf-node.llnl.gov/search/cmip5/

Table S2 Descriptions of ground phenological data.

Species	Number of sites	Number of observations	Dates of autumn foliar senescence (day of year)
Aesculus hippocastanum	2034	48288	263±11
Betula pendula	1919	45931	281±14
Betula pubescens	20	468	275±20
Fagus sylvatica	1794	42502	284±14
Populus tremula	14	230	262±11
Quercus robur	1792	42304	288±13
Sorbus aucuparia	101	1320	275±17
Tilia cordata	123	2402	286±19
Total	2405	183448	273±25

Table S3 Descriptions of flux sites data.

Site ID and Ref.	Site Name	Country	PFT	Lat (°)	Lon (°)	Alt (m)	Time range
BE-Bra[1]	Brasschaat	Belgium	MF	51.30761	4.51984	16	1999-2014
BE-Vie[2]	Vielsalm	Belgium	MF	50.3051	5.9981	493	1996-2014
CA-Man[3]	Manitoba - Northern Old Black Spruce	Canada	ENF	55.8796	-98.4808	259	1994-2008
CA-Oas[4]	Saskatchewan - Western Boreal, Mature Aspen	Canada	DBF	53.6289	-106.198	530	1996-2010
CA-Obs[5]	Saskatchewan - Western Boreal, Mature Black Spruce	Canada	ENF	53.9872	-105.118	629	1999-2010
DE-Gri[6]	Grillenburg	Germany	GRA	50.95	13.5126	385	2004-2014
DE-Hai[7]	Hainich	Germany	DBF	51.0792	10.453	430	2000-2012
DE-Lnf[8]	Leinefelde	Germany	DBF	51.3282	10.3678	451	2000-2012
DE-Tha[9]	Tharandt	Germany	ENF	50.9624	13.5652	385	1997-2014
DK-Sor[10]	Soroe	Denmark	DBF	55.4859	11.6446	40	1996-2014
DK-ZaH[11]	Zackenberg Heath	Denmark	GRA	74.4732	-20.5503	38	2000-2014
FI-Hyy[12]	Hyytiala	Finland	ENF	61.8474	24.2948	181	1996-2014
FI-Sod[13]	Sodankyla	Finland	ENF	67.3619	26.6378	180	2001-2014
NL-Loo[14]	Loobos	Netherlands	ENF	52.1666	5.7436	25	1996-2012
RU-Cok[15]	Chokurdakh	Russia	OSH	70.8291	147.4943	48	2003-2013
RU-Fyo[16]	Fyodorovskoye	Russia	ENF	56.4615	32.9221	265	1998-2014
RU-Sam[17]	Samoylov	Russia	GRA	72.3738	126.4958	-	2002-2014
US-Atq[18]	Atqasuk	America	WET	70.4696	157.4089	15	1999-2008

Supplementary references

1. Carrara A, Janssens IA, Yuste JC, Ceulemans R (2004) Seasonal changes in photosynthesis, respiration and NEE of a mixed temperate forest. *Agric For Meteorol* **126**:15–31.

2. Aubinet M, et al. (2001) Long term carbon dioxide exchange above a mixed forest in the Belgian Ardennes. *Agric For Meteorol* **108**:293–315.

3. Amiro BD, et al. (2006) Carbon, energy and water fluxes at mature and disturbed forest sites, Saskatchewan, Canada. *Agric For Meteorol* **136**:237–251.

4. Black TA, el al. (1996) Novak Annual cycles of water vapor and carbon dioxide fluxes in and above a boreal aspen forest. *Glob Change Biol* **2**:219-229.

5. Black TA, el al. (1996) Novak Annual cycles of water vapor and carbon dioxide fluxes in and above a boreal aspen forest. *Glob Change Biol* **2**:219-229.

6. Prescher AK, Grünwald T, Bernhofer C (2010) Land use regulates carbon budgets in eastern Germany: From NEE to NBP. *Agri. For Meteorol* **150**:1016-1025.

7. Knohl A, Schulze ED, Kolle O, Buchmann N (2003) Large carbon uptake by an unmanaged 250-year-old deciduous forest in Central Germany. *Agric For Meteorol* **118**:151–167.

8. Anthoni PM, et al. (2004) Forest and agricultural land-use-dependent CO_2 exchange in Thuringia, Germany. *Glob Change Biol* **10**:2005–2019.

9. Grünwald T, Bernhofer C (2007) A decade of carbon, water and energy flux measurements of an old spruce forest at the Anchor Station Tharandt. *Tellus B Chem Phys Meteorol* **59**:387-396.

10. Pilegaard K, Ibrom A, Courtney MS, Hummelshøj P, Jensen NO (2011) Increasing net CO_2 uptake by a Danish beech forest during the period from 1996 to 2009. *Agric For Meteorol* **151**:934-946.

11. Lund M, et al. (2012) Trends in CO_2 exchange in a high Arctic tundra heath, 2000-2010. *J Geophys Res* **117**:G02001.

12. Suni T, et al. (2003) Long-term measurements of surface fluxes above a Scots pine forest in Hyytiälä, southern Finland, 1996-2001. *Boreal Env Res* **8**:287-301.

13. Thum T, et al. (2007) Parametrization of two photosynthesis models at the canopy scale in a northern boreal Scots pine forest. *Tellus B Chem Phys Meteorol* **59**:874-890.

14. Moors EJ (2012) Water Use of Forests in The Netherlands, PhD-thesis, Vrije Universiteit Amsterdam., the Netherlands.

15. Van der Molen MK, et al. (2007) The growing season greenhouse gas balance of a continental tundra site in the Indigirka lowlands, NE Siberia. *Biogeosciences* **4**:985-1003.

16. Kurbatova J, Varlagin A, Xiao X, Vygodskaya N (2008) Modeling carbon dynamics in two adjacent spruce forests with different soil conditions in Russia. *Biogeosciences* **5**:969-980.

17. Boike J, et al. (2013) Baseline characteristics of climate, permafrost and land cover from a new permafrost observatory in the Lena River Delta, Siberia (1998-2011). *Biogeosciences* **10**:2105-2128.

18. Donatella Z, Walt O (2003-2008) FLUXNET2015 US-Atq Atqasuk, Dataset. https://doi.org/10.18140/FLX/1440067